Propagation behaviors of the rotating detonation wave in kerosene-air two-phase mixtures with wide equivalence ratios

Zhaoxin Ren[a], Yan Sun[b], Bing Wang[c]

[a] *Zienkiewicz Centre for Computational Engineering, Faculty of Science and Engineering, Swansea University, Swansea, SA1 8EN, UK*

[b] *School of Power and Energy, Northwestern Polytechnical University, Xi'an, 710072, China*

[c] *School of Aerospace Engineering, Tsinghua University, Beijing, China, 100084*

Abstract

Rotating detonation engine (RDE) with pressure gain is innovative for propulsion. To evaluate the RDE using liquid fuel, the rotating detonation wave (RDW) with kerosene droplets is numerically studied. The Eulerian-Lagrangian two-phase flow model is applied to predict the propagation features of the RDW and the quenching phenomenon. A hybrid WENO scheme is used to capture the shock/detonation wave and a reduced reaction model is applied. This research analyzes the influence of the equivalence ratio on the dynamics of propagation and quenching of RDW by applying comparative simulations with liquid kerosene and pre-evaporated kerosene. The focus is fixed on the stable operation limits as a function of the equivalence ratio. The results under the present conditions show that the RDWs formed in the two-phase mixtures have a narrower stable propagation regime of the equivalence ratio than that of the RDWs fueled with pre-evaporated kerosene. The difference between the gaseous and two-phase RDWs becomes obvious under the fuel-rich conditions, and the RDW is strengthened in the gaseous flow but is weakened in the two-phase mixture. The change of the kerosene fuel from vapors to droplets results in a bifurcated wave structure near the inlet due to the interactions among droplets, shock waves, and flame. For the quenching mechanism, the fuel-lean quenching is from the lack of reactive mixtures from the droplet evaporation near the inlet, and the fuel-rich quenching is attributed to the absence of the transverse waves from the triple point. The comparative study shows that the fuel-rich injection is more suitable to generate stable RDWs within the present initial conditions.

Keywords: Rotating detonation wave, Two-phase, Equivalence ratio, Propagation, Quenching.

List of abbreviation

RDW	rotating detonation wave	RDE	rotating detonation
RDC	rotating detonation combustor	C-J	engine Chapman-Jouguet
RANS	Reynolds-averaged Navier-Stokes	CD	computation domain
OSW	oblique shock wave	LPTW	left-propagating transverse wave
RPTW	right-propagating transverse wave		

1 Introduction

Researchers have been seeking novel technologies to improve the performance of aerospace propulsion systems. Compared with the combustion mode of deflagration in traditional aerospace engines, the detonation raised researchers' attention in recent years since it can achieve a fast reaction rate with pressure-gain combustion and the detonation-based engine is expected to have a high thermodynamic cycle efficiency. As one type of the organization of detonation, the rotating detonation received a wide research focus recently [1-4]. The detonation wave is initiated in an annular/hollow combustion chamber and propagates along the circumferential direction in the chamber. The rotating detonation wave (RDW) consumes the reactive mixture and can rotate continuously and stably under certain conditions. Some aspects of the RDW-based engine, namely the rotating detonation engine (RDE), have been studied both experimentally and numerically, such as the injection of fuel to the rotating detonation combustor (RDC) [5, 6], mixing process [7, 8], initiation of RDW [9, 10], propagation mode of RDW [11, 12], and the performance of thrust/impulse of RDE [13].

For various parameters of the combustor affecting the propagation features of RDW, the fuel-air equivalence ratio plays a significant role that contributes to the detonation stability in RDE. In particular, the initiation ability of the rotating detonation and the heat release rate, associated with the wave propagation velocity of RDW and pressure-gain features, will have different changing trends as the equivalence ratio varies. Liu et al. [14] found that the change of the equivalence ratio affects the detonation wave velocity as well as the propagation mode of hydrogen-air RDW. Wang et al. [15] conducted experimental and numerical studies on the hydrogen/oxygen RDW, and they concluded that the dependence of RDW propagation velocity on equivalence ratio displays a non-uniform curve, associated with the equivalence ratio around 0.5 leads to a maximum propagation velocity. Anand et al. [16] indicated that the airflow rate and equivalence ratio influence the detonation-induced pressure rise in the RDE fueled with hydrogen-air mixtures. Fotia et al. [17] analyzed the effects of nozzle configurations

of RDE using hydrogen fuel, and the results showed that the specific thrust and specific impulse increase with the increasing equivalence ratio. Deng et al. [18] experimentally investigated the influence of mass flow rate and equivalence ratio. The results indicated that the dependence of wave speed on the equivalence ratios has a relationship with the airflow rate, and the rotating detonation stability is enhanced as the equivalence ratio increases. Xie et al. [19] concluded four propagation modes of the hydrogen-air RDW as the equivalence ratio changes under the fuel-lean conditions. They [20] also found that the stable propagation limit is broadened as the airflow rate as well as oxygen volume fraction increases for an oxygen-enriched hydrogen-fueled RDW. Li et al. [21] studied that the initiation of RDW is expected to have a shorter time as the hydrogen-oxygen equivalence ratio increases, associated with the variation of propagation mode. The maximum frequency and maximum wave velocity occurred at the equivalence ratio of 1.0.

In the related studies on RDE, most of the research considered gaseous fuel including hydrogen, methane, and ethylene. Recently, the liquid fuel for RDE has attracted scholars' interest. The liquid fuel has more advantages over the gaseous fuel for engineering applications. Kindracki [22] used liquid kerosene and added hydrogen in the RDC to enhance the detonation. Compared to the Chapman-Jouguet (C-J) values, the experimental data showed that the velocity of the RDW has a 20-25% decrease. Frolov et al. [23] performed the measurements on the rotating detonation of the hydrogen-liquid propane-air mixture and clarified the effects of hydrogen on the RDW. Then they used the liquid fuel film to produce the RDWs [24]. Zheng et al. [25] used the preheated oxygen-enriched air as the oxidizer and studied the RDW fueled with liquid kerosene. They kept the equivalence ratio at 0.81 but changed the total temperature of the air. They found that there are detonation instability, mode transition, and re-initiation in their experiments, and indicated that the instability is due to the interaction between RDW and the supply plenum. Zhao et al. [26] analyzed the effects of the nozzle convergent ratio on the RDW using liquid kerosene and found three propagation modes. The increasing convergent ratio accelerates the formation of the RDW and the small ratio contributes to the stable RDW. Meng et al. [27] the RDW of liquid kerosene in air-breathing mode and the equivalence ratio varied. A 60% C-J velocity is obtained in the cavity-based combustor. Xu et al. [28] applied liquid kerosene and oxygen-rich air for the RDW. They studied the effects of injection area ratio and found that a reducing injection area leads to an increase in pressure and velocity of detonation waves. Cheng et al. [29] conducted a large-scale experiment for the kerosene RDW and found the velocity of RDW increased with the increase of the equivalence ratio from 0.85 to 1.0. Ma et al. [30] carried out the experiments on

the RDW of gasoline and the velocity and pressure of the RDWs increased with the increase of equivalence ratio and air temperature.

For the numerical simulation of the two-phase RDW using liquid fuel. Hayashi et al. [31] investigated the detonation features of the JP-10 liquid fuel and applied a series of validations using a two-step reduced reaction mechanism. They analyzed the influence of the fuel droplet size and the droplet vaporization on the propagation of RDW. Meng et al. [32] utilized a mixture of partially pre-vaporized n-heptane and hydrogen as the fuel. The one-step reaction model was applied. The increasing pre-vaporization level and the decreasing droplet size will contribute to stable detonation. Wang and Weng [33] used the Euler-Euler model to study the kerosene-air RDW and considered the influence of total temperature and droplet size. The increase of total temperature suppresses the total pressure gain performance. Salvadori et al. [34] analyzed the effects of kerosene droplets on the performance of hydrogen rotating detonation and the addition of kerosene can add heat release. Wang et al. [35] used the RANS approach to simulate the rotating detonation of liquid $C_{12}H_{23}$ with different pre-heated temperatures. Huang and Lin [36] simulated the RDW in a fuel-rich mixture of hydrogen, liquid kerosene, and air based on OpenFOAM@.

In general, the experiments on the two-phase RDW seem to lack information on the atomization and the initial spray features of the liquid fuel, and the details of fuel dispersion and the interphase interaction are not observed due to the limitation of measurements. The detailed simulation of two-phase RDW is challenging due to the complex interactions of droplets, shock waves, and exothermic reactions, which needs to use high-order numerical schemes with fine meshes. The liquid fuel needs to form vapors to mix with oxygen before the chemical reaction starts. The transition from liquid to gas is complex considering the inter-phase transfers of mass, momentum, and heat. The underlying physics in the complex two-phase system needs to be studied and the mechanics of the two-phase reacting flow influence the RDW propagation features, and relative knowledge is still lacking. The purpose of this study is to enhance the understanding of the rotating detonation structure using liquid fuel via high-fidelity numerical simulations. The effects of the equivalence ratio in a wide range are investigated. The mechanisms of propagation and quenching of the RDW are analyzed. In the next section, the simulation configuration and numerical details are provided.

2 Mathematical and physical models

The present numerical simulations solve the conservative equations of mass, momentum, and total energy as well as the transport equations of chemical species needed for the combustion process. Every dispersing fuel droplet is tracked individually along its Lagrangian path. The inter-phase coupling between the Eulerian reacting flow and the Lagrangian droplets is considered by a point-source in cell (PSIC) method [37]. The mathematical equations used in the present simulations are as below,

$$\text{gas-phase equations}\begin{cases} \dfrac{\partial}{\partial t}(\rho)+\dfrac{\partial}{\partial x_j}\left(\rho u_j\right)=S_{\mathrm{m}} \\ \dfrac{\partial}{\partial t}\left(\rho u_i\right)+\dfrac{\partial}{\partial x_j}\left(\rho u_i u_j+P\delta_{ij}-\tau_{ij}\right)=S_{\mathrm{F},i} \\ \dfrac{\partial}{\partial t}\left(\rho e_{\mathrm{t}}\right)+\dfrac{\partial}{\partial x_j}\left(\left(\rho e_{\mathrm{t}}+P\right)u_j-u_i\tau_{ij}-q_j\right)=S_{\mathrm{Q}} \\ \dfrac{\partial}{\partial t}\left(\rho Y_k\right)+\dfrac{\partial}{\partial x_j}\left(\rho Y_k u_j\right)+\dfrac{\partial}{\partial x_j}\left(\rho Y_k\left(V_{k,j}+V_j^{\mathrm{c}}\right)\right)=S_{\mathrm{combustion},k}+S_{Y_k} \end{cases} \tag{1}$$

$$\text{droplet-phase equations}\begin{cases} \dfrac{\mathrm{d}x_{\mathrm{d},i}}{\mathrm{d}t}=u_{\mathrm{d},i} \\ \dfrac{\mathrm{d}u_{\mathrm{d},i}}{\mathrm{d}t}=\dfrac{F_{\mathrm{d},i}}{m_{\mathrm{d}}}=\dfrac{F_{\mathrm{sg},i}+F_{\mathrm{qs},i}+F_{\mathrm{am},i}+F_{\mathrm{vu},i}}{m_{\mathrm{d}}} \\ \dfrac{\mathrm{d}T_{\mathrm{d}}}{\mathrm{d}t}=\dfrac{Q_{\mathrm{d}}+\dot{m}_{\mathrm{d}}L_{\mathrm{V}}}{m_{\mathrm{d}}c_{\mathrm{L}}}=\left(\dfrac{f_{\mathrm{Q}}\left(\mathrm{Re}_{\mathrm{d}}\right)}{\tau_{\mathrm{a}}}\right)\left(\dfrac{\mathrm{Nu}}{3\,\mathrm{Pr}}\right)\left(\dfrac{c_p}{c_{\mathrm{L}}}\right)\left(T_{@\mathrm{d}}-T_{\mathrm{d}}\right)+\left(\dfrac{\dot{m}_{\mathrm{d}}}{m_{\mathrm{d}}}\right)\dfrac{L_{\mathrm{V}}}{c_{\mathrm{L}}} \\ \dfrac{\mathrm{d}m_{\mathrm{d}}}{\mathrm{d}t}=\dot{m}_{\mathrm{d}}=-m_{\mathrm{d}}\left(\dfrac{1}{\tau_{\mathrm{a}}}\right)\left(\dfrac{\mathrm{Sh}}{3\mathrm{Sc}}\right)\mathrm{In}\left(1+B_{\mathrm{M}}\right) \end{cases} \tag{2}$$

$$\text{inter-phase coupling terms}\begin{cases} S_{\mathrm{m}}=-\dfrac{1}{\Delta V}\sum_{N_{\mathrm{c}}}\left(\dot{m}_{\mathrm{d}}\right) \\ S_{\mathrm{F},i}=-\dfrac{1}{\Delta V}\sum_{N_{\mathrm{c}}}\left(F_{\mathrm{d},i}+\dot{m}_{\mathrm{d}}u_{\mathrm{d},i}\right) \\ S_{\mathrm{Q}}=-\dfrac{1}{\Delta V}\sum_{N_{\mathrm{c}}}\left(Q_{\mathrm{d}}+\dot{m}_{\mathrm{d}}\left(\dfrac{u_{\mathrm{d},i}u_{\mathrm{d},i}}{2}+h_{\mathrm{V,sf}}\right)\right) \\ S_{Y_k}=\begin{cases} -\dfrac{1}{\Delta V}\sum_{N_{\mathrm{c}}}\left(\dot{m}_{\mathrm{d}}\right) & \text{for fuel} \\ 0 & \text{for other species} \end{cases} \end{cases} \tag{3}$$

The density, velocity vector, static pressure, static temperature, and total energy of the gas-phase are represented by ρ, u_i, P, T, and e, respectively, in the above equations. The Y_k indicates the mass fraction of species k in the mixture. The kinetic theory [38] is applied to model the transportation parameters including the dynamics viscosity, heat conductivity coefficient, and mass diffusion coefficient. The fuel droplets are tracked and a sparse dispersion of the droplet-phase system is assumed. The unsteady forces from the gas-phase to the droplet are modeled by adding the stress-gradient, quasi-steady, added-mass, and viscous-unsteady forces [39] to the

momentum equation of the droplet-phase. The definitions of the parameters in the above governing equations for the gas-phase and droplet-phase can be found in Ref. [40].

The two-phase reacting flow is solved by our in-house code, and this code has been applied for the numerical investigation of two-phase reacting flow [40] and two-phase detonation [41]. The high-order numerical scheme of WENO-CU6 [42] is coupled with the code to obtain a sixth-order accuracy for the convection term. The diffusion term is discretized by a six-order compact scheme. A third-order Runge-Kutta integration is used to get the new physical information of the droplet-phase. A fourth-order Lagrangian interpolation method is applied to pick up the physical information at the droplet's position from the flow field. The time integration for the droplet-phase is a third-order Adams-Bashforth method.

The combustion of kerosene fuel and air is utilized as a two-step mechanism considering the reduction of the computational costs [43]. Kerosene contains the components such as $C_{10}H_{22}$, C_9H_{12}, C_9H_{18}, et al., which can be approximated as $C_{10}H_{20}$ according to their mass fractions. This combustion model has a fuel-consumption step from kerosene to CO and H_2O, followed by the oxidation step from CO to CO_2, as follows,

$$C_{10}H_{20} + 10O_2 \Rightarrow 10CO + 10H_2O \tag{4a}$$

$$CO + 0.5O_2 \Leftrightarrow CO_2 \tag{4b}$$

Eq. (4a) is the irreversible reaction of kerosene and Eq. (4b) shows the equilibrium reaction of CO and CO_2. Their forward reaction rates, k_1 and k_2, are written as,

$$k_1 = A_1 f_1(\phi) \exp(-E_1 / RT)[\mathrm{KERO}]^{n_{\mathrm{KERO}}}[\mathrm{O_2}]^{n_{\mathrm{O_2},1}} \tag{5a}$$

$$k_2 = A_2 f_2(\phi) \exp(-E_2 / RT)[\mathrm{CO}]^{n_{\mathrm{CO}}}[\mathrm{O_2}]^{n_{\mathrm{O_2},2}} \tag{5b}$$

where A is the pre-exponential factor, E is the activation energy, and n is the reaction order. f_1 and f_2 are the correction functions for the reaction rate based on the equivalence ratio Φ. The details of these parameters can be found in Ref. [43]. The reaction mechanism together with the simulation code is validated the ability to predict the propagation velocity and cell size of the detonation wave. Fig. 1 shows the detonation wave velocity, U_D, and the cell size, λ, which are calculated by our in-house code for the mixture with different equivalent ratios. The results are compared with the experiment [44]. The numerical and experimental results show reasonably good consistency.

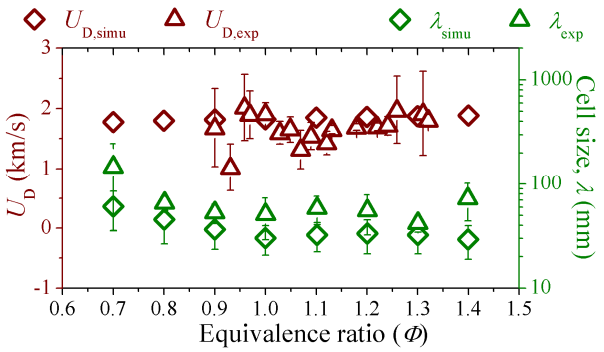

Fig. 1 The comparison of detonation velocity, U_D, and cell size, λ, predicted by present numerical simulations (brown scatters) and experiments (green scatters).

The two-phase rotating detonation is simulated in a two-dimensional plane in the present study. The previous research indicated that the key features of the RDW itself have a slight difference from the two-dimensional (2D) and three-dimensional (3D) simulations [31]. A 3D annular model combustor is unwrapped and a 2D computation domain (CD) is scaled by the black dashed lines, as shown in Fig. 2. The periodic boundaries are set for the upper and lower boundaries, as indicated in Fig. 2. The airflow laden with dispersed fuel droplets (black dots) enters the CD from the left boundary. The variable cross-section inlet nozzle model is applied and the inlet velocity is calculated from the local pressure, as proposed by Fievisohn et al. [46]. The total pressure loss resulting from the nozzle expansion is considered in this model and the nozzle area ratio is 1/3.

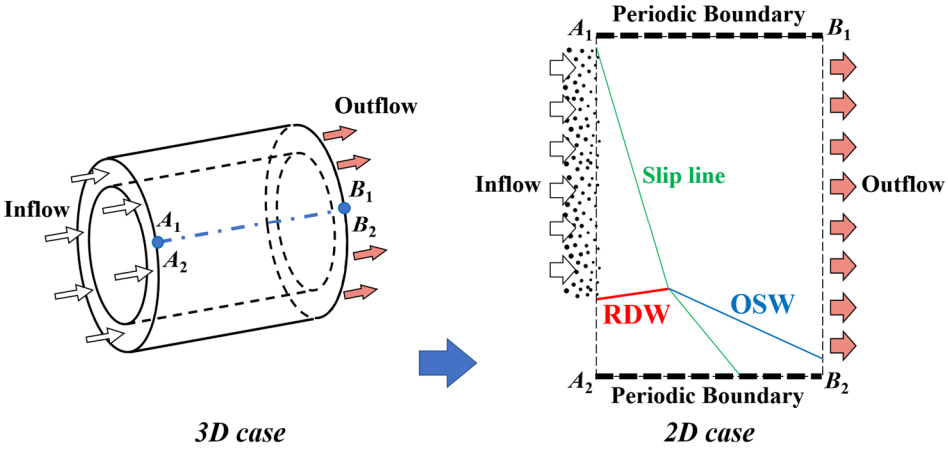

Fig. 2 Schematic of rotating detonation waves formed in the two-phase mixture.

The initiation of RDW should be properly set to achieve the one-way propagation, and the present investigation uses the initiation method in Ref. [47]. As shown in Fig. 3, the initial computation domain is divided into four parts. Regime 1 is filled with a mixture of pre-evaporated kerosene vapors and air with normal temperature and pressure. Regime 3 and Regime 4 are the air with normal temperature and pressure. Regime 2 is the air with high

temperature and pressure for the initiation of detonation. The static temperature is 3000 K, and the distribution of the static pressure is as follows,

$$P = \left[29\left(\frac{y - y_1}{y_2 - y_1} \right)^2 + 1 \right] \text{ atm} \tag{6}$$

where y_1 and y_2 are the transverse locations of the lower and upper boundaries of Regime 2. The dimension of CD is 0.06 m in the y-direction and 0.04 m in the x-direction. The detonation wave generally propagates from the bottom to the top.

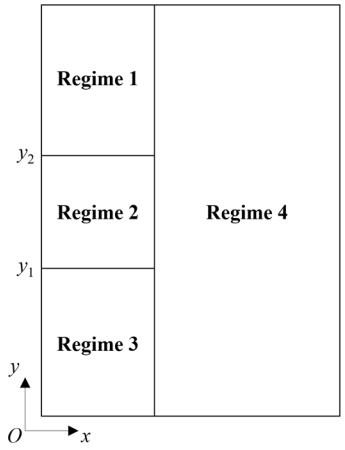

Fig. 3 Schematic of initial conditions.

The inlet parameters use total pressure P_0, and total temperature, T_0, to calculate the needed parameters for the simulations. In the present study, the P_0 is 7 atm and the T_0 is 1000 K, calculated by an air-breathing vehicle with a flight Mach number of 4.5 and a flight altitude equaling 25 km. The pre-atomized fuel droplets are used. The initial droplet velocity, u_{d0}, is equal to the velocity of the airflow, and the initial diameter of the kerosene droplet is d_{d0} = 2 μm. The initial temperature of the droplet is chosen as room temperature (298.15 K). For evaluating the equivalence ratio of the inflow two-phase mixture, a parameter Φ_s is used. Φ_s is represented by $\Phi_s \cdot (\mathrm{F/O})_{st} = \dot{m}_{fuel} / (\dot{m}_{air} Y_{O_2})$. Here, $(\mathrm{F/O})_{st}$ is the stoichiometric fuel-to-oxidizer ratio and equals 3.4 for kerosene. $\dot{m}_{fuel}$ and $\dot{m}_{air}$ are the mass flow rates of fuel and ai, and Y_{O_2} = 0.23 is the mass fraction of oxygen. The Φ_s increases from 0.8 to 1.6 to analyze the effects. Table 1 summarizes the simulation cases for two-phase rotating detonation.

Table 1 Simulation cases of two-phase RDW.

Case #	RDF1	RD	RDF2	RDF3	RDF4
$\boldsymbol{\Phi_s}$	0.8	1.0	1.2	1.4	1.6

A series of simulation cases by using pre-evaporated kerosene vapors as the fuel is also performed to quantify the difference between the gas-phase and two-phase rotating detonations, and the equivalence ratio for the reactive mixture of fuel vapors and air, Φ_0, varies from 0.6 to 1.8. Table 2 provides the cases for simulating the gas-phase RDW.

Table 2 Simulation cases of gas-phase RDW.

Case #	RF0	RF1	R	RF2	RF3	RF4	RF5
$\boldsymbol{\Phi_0}$	0.6	0.8	1.0	1.2	1.4	1.6	1.8

The computational grid for the two-phase reacting flow and detonation needs to meet the requirements of the particle-in-cell model as well as the resolution of the detonation wave structure. The grid independence analysis is applied for the simulation of rotating detonation. Case R with a stoichiometric mixture of kerosene vapors and air is calculated using three grid sizes (25 μm, 50 μm, and 100 μm). Fig. 4 shows the results from three sets of grids. It is found that the main wave structures of the flow field for three grid sizes are similar. The fine unsteady waves on the front of RDW cannot be predicted by the largest grid Δ = 100 μm. Therefore, the grid size Δ = 50 μm is chosen in this study. On one side, the ratio of the grid to droplet size, Δ / d_{d0} > 10, meets the criterion of the particle-in-cell model and can get correct droplet dynamics. On the other hand, the cell size of the kerosene-air detonation wave can contain around 1000 grids [31] and can provide a good resolution of the wave structure of the kerosene-air detonation.

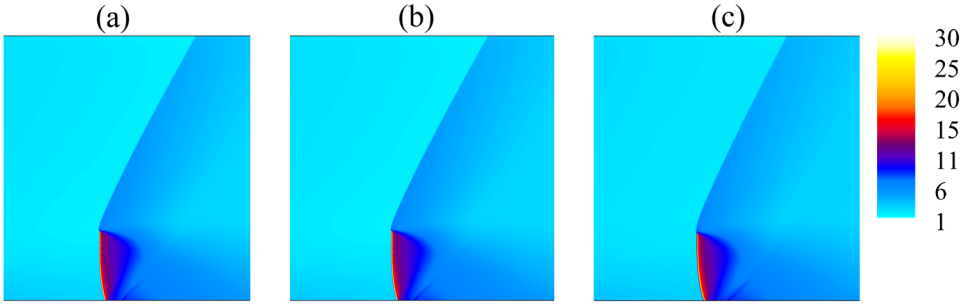

Fig. 4 Pressure (atm) distributions with grid sizes: (a) Δ = 25 μm, (b) Δ = 50 μm, (c) Δ = 100 μm.

3 Rotating detonation of kerosene vapors

The pre-evaporated kerosene vapors are first utilized as the fuel and the effects from the evaporation of the dispersing droplets on RDW are not considered. For the fuel-lean conditions, the Case RF0 with Φ_0 = 0.6 cannot

achieve a stable propagation of detonation wave and the quenching occurs during the first rotating circle. The quenching dynamics are shown in Fig. 5 and Fig. 6 by the temporal distributions of the pressure and temperature, respectively. The detonation wave is initiated and propagates from bottom to top. The initial RDW has a smooth front, as depicted in Fig. 5(a). It is found that the wave front near the inlet becomes curved as the detonation wave traverses the fuel-lean reactive mixtures, associated with the decreasing temperature of the combustion products, as seen in Fig. 5(b) and Fig. 6(b). This is mainly because the heat release is suppressed due to the fuel-lean chemical reaction as the flame interacts with the incoming reactive mixtures. The curved region on the detonation front further expands with unsteady transverse waves as the fuel-lean mixture is injected into the flow field continuously. The decoupling of shock and flame generates from the inlet, as scaled by the white dashed lines in Fig. 5(d). From the temperature distributions, the low-temperature regime enlarges continuously, which is attributed to the weak chemical reaction. The height of RDW decreases continuously from Fig. 5(d) to Fig. 5(e). Finally, the detonation front with high pressures disappears. As seen in Fig. 5(f), there is only a curved shock wave with a V-shape in the flow field. The unreacted mixtures from the inlet start to fill in the flow field, as depicted in Fig. 6(f).

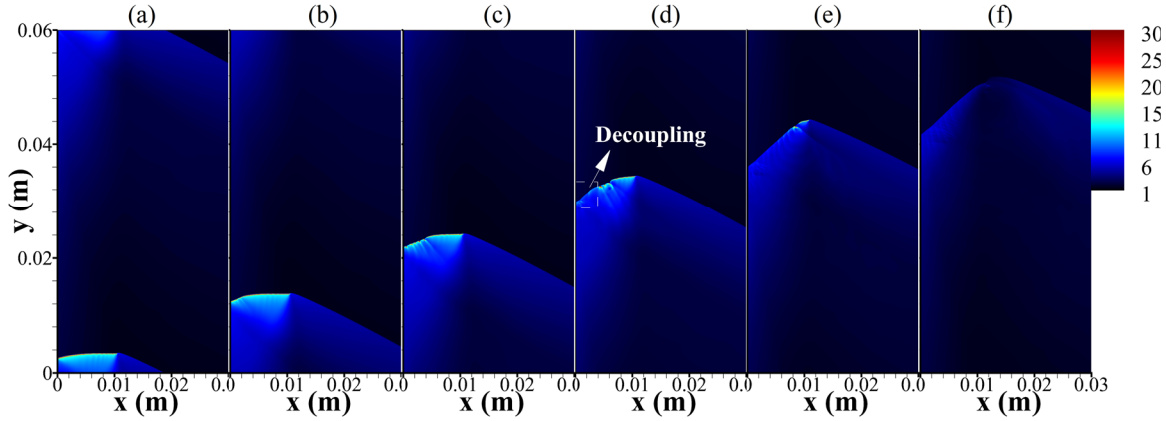

Fig. 5 Temporal evolution of pressure (atm) distribution for Case RF0 (Φ_0 = 0.6: (a) τ_0 μs, (b) τ_0 + 6 μs, (c) τ_0 + 12 μs, (d) τ_0 + 18 μs, (e) τ_0 + 24 μs, and (f) τ_0 + 30 μs.

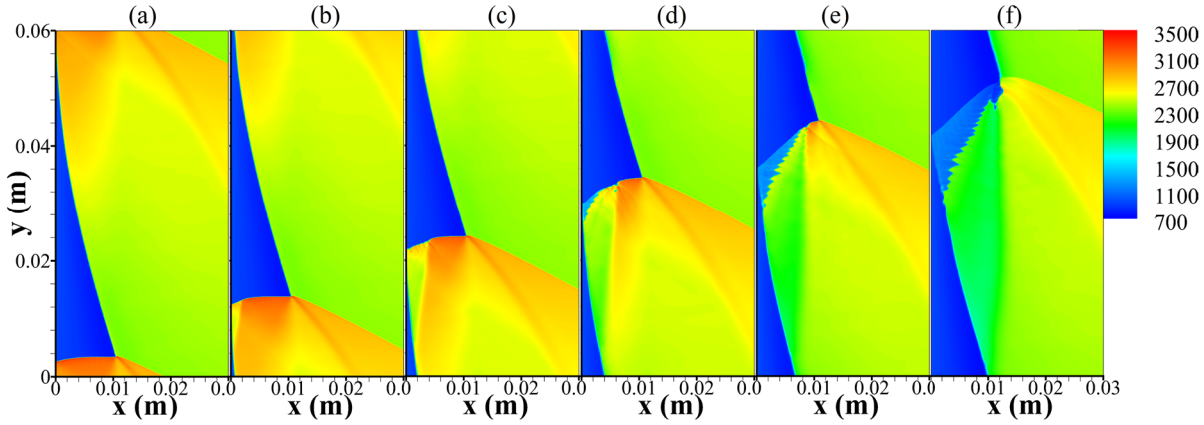

Fig. 6 Temporal evolution of temperature (K) distribution for Case RF0 (Φ_0 = 0.6): (a) τ_0 μs, (b) τ_0 + 6 μs, (c) τ_0 + 12 μs, (d) τ_0 + 18 μs, (e) τ_0 + 24 μs, and (f) τ_0 + 30 μs.

For the fuel-rich premixing inflow, the quenching of rotating detonation occurs for Case RF5 with Φ_0 = 1.8. The quenching dynamics, associated with the temporal evolution of the wave structures, are similar to those of Case RF0. The quenching of detonation is first generated from the inlet owing to the extremely fuel-rich mixtures and the associated suppression of exothermic reaction. Subsequently, the quenching regime expands towards the outlet, and the height of the detonation front becomes short. Finally, it is observed the detonation wave cannot sustain the continuous rotation and the detonation front breaks down.

The stable RDWs are formed for the equivalence ratios from 0.8 to 1.6 in the present study. Fig. 7 displays the instantaneous distributions of pressure at the same time for these cases. From the transverse locations of the RDW, it is observed that the increase of the Φ_0 leads to a faster propagation of detonation waves. The variation of Φ_0 not only has an influence on the propagation features of RDW but affects the detonation wave structures. In particular, for the increase of Φ_0 from Case RF2 to Case RF3 (Φ_0 from 1.2 to 1.4), the pressure of the RDW is observed to increase and the wave front becomes smooth. The fuel-rich premixing inflows lead to the unsteady transverse waves formed on the front of the RDW, as depicted in Fig. 7(e). With the increases of Φ_0 from 0.8 to 1.0, the RDW propagates faster and the detonation is strengthened with the increase of wave pressure, which is attributed to the enhancement of the exothermic reaction. In addition, the part of the detonation surface near the triple point tends to be corrugated with a concave shape, as shown in Fig. 7(b). As the equivalence ratio rises to 1.6 for Case RF4 after the smooth detonation fronts for cases RF2 and RF3, the rotating detonation becomes unstable, as shown by the fine transverse waves on the front in Fig. 7(e).

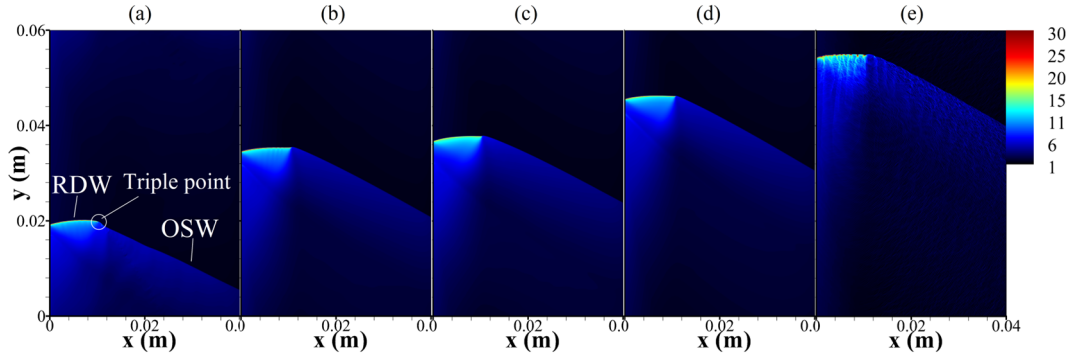

Fig. 7 Instantaneous distributions of pressure (atm) for (a) Case RF1 (Φ_0 = 0.8), (b) Case R (Φ_0 = 1.0), (c) Case RF2 (Φ_0 = 1.2), (d) Case RF3 (Φ_0 = 1.4), and (e) RF4 (Φ_0 = 1.6) at a same time.

The pressure variations at chosen observation point (x = 2 mm, y = 50 mm) are provided in Fig. 8 to illustrate the propagation behaviors of the RDW. Generally, it is found that the velocities of detonation waves increase with the increase of equivalence ratio from 0.8 to 1.6, associated with the stronger detonation wave. In particular, the wave pressure for Case R (Φ_0 = 1.0) is higher than that of Case RF2 (Φ_0 = 1.2) with a higher fuel mass loading, which corresponds to the smooth front of RDW and the low wave pressure in Fig. 7(c). The detonation wave for the fuel-lean case (Case RF1 and Φ_0 = 0.8) and the fuel-rich case (Case RF4 and Φ_0 = 1.6) are unstable, represented by the large fluctuations of the pressure peaks in Fig. 8(a). This is attributed to the unsteady transverse waves and their evolutions on the detonation front, as shown in Fig. 7(a) and Fig. 7(e).

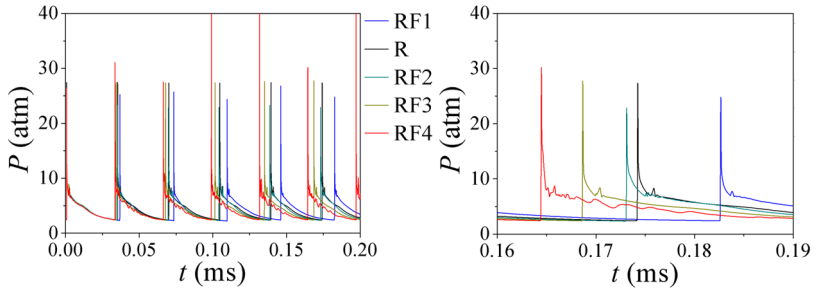

Fig. 8 Variation of pressure at the observation point: (left) five rotating circles and (right) local enlargement.

4 Rotating detonation of kerosene droplets

For the fine droplets considered in the present study, the main effects on the rotating detonation are from their finite evaporation rates and the associated cooling process in the carrier flow. The RDW cannot sustain the continuous propagation as the spray equivalence ratio, Φ_s, decreases to 0.8 or increases to 1.6, which shows that the stable operation regime of two-phase RDW for the equivalence ratio is narrow than that of RDW using pre-evaporated kerosene vapors. The detailed analysis is given in the following part.

The two-phase RDWs can achieve self-sustained propagation within the stable operation regime for the spray equivalence ratio from 1.0 to 1.4 under the present inflow conditions. The stable RDWs are formed in the fuel-rich mixtures. Fig. 9 shows the pressure distributions for cases RD, RDF2, and RDF3 at the same time. The change from fuel vapors to droplets has an obvious influence on the wave structures of rotating detonation. A short detonation wave, referred to as FRDW in Fig. 9(a), is generated near the inlet, associated with an oblique shock wave, as shown in Fig. 9(a). Another detonation wave with a longer height is generated in the downstream regime, as indicated by RDW, and it is the main detonation wave for consuming the reactive mixtures in the combustor.

For the structures, the unsteady transverse waves are formed on surface of the RDW. In particular, the portion near the inlet is curved to connect with the FRDW at the inlet and becomes a non-reacting shock wave. The RDW and FRDW display a bifurcated wave structure. This structure is mainly because the dispersing fuel droplets from the inlet cannot finish the evaporation to generate enough vapors for the exothermic reaction, and the leading shock wave decouples with the flame. Then the leading shock propagates to traverse the two-phase mixture. The heating from the shock contributes to the evaporation of the fuel droplets. Subsequently, more fuel vapors are generated to form the reactive mixtures for combustion and the detonation wave (FRDW) is formed at the inlet. Compared with the main wave (RDW), the FRDW tends to be much shorter, which is due to the lack of reactive mixture to establish a continuous flame. The distance between the RDW and the FRDW becomes close with the increase of the spray equivalence ratio to 1.2 for Case RDF2. This is mainly because more fuel droplets are injected and hence the exothermic reaction is enhanced, which results in the coupling of shock and flame as well as the FRDW in an earlier time. The detonation surface of RDW tends to be smooth, as shown by the disappearance of transverse waves on the wavefront in Fig. 9(b). For Case RDF3 with $\Phi_s = 1.4$, the RDW moves faster as more fuel droplets are injected into the flow. The leading RDW is away from the FRDW, and the bifurcated wave structure is similar to that of Case RD. The front of the RDW becomes unstable with unsteady cellular structures.

Fig. 10 provides the instantaneous distributions of gas temperature for cases RD, RDF2, and RDF3 at the same time. Here, the black dashed lines indicate the fuel vapors that are not consumed during detonation. The variation of the spray equivalence ratio has an influence on the temperature fields of the combustion product. As shown in Fig. 10(a), the combustion products from the detonation wave are separated from the former combustion products via a slip line. The shearing vortices are formed along the slip line because of the velocity difference. There are unreacted fuel vapors after the detonation waves, and the amount enlarges with the increasing equivalence ratio, as shown by the spatial distribution of the Y_F. With the increase of the fuel droplet loading, the number of unreacted

mixtures is found to enlarge, as depicted in Fig. 11. In particular, for Case RDF3, a large number of unburned fuel vapors exist in the combustor. Most of them are generated from the near-inlet curved shock as the shock-induced deflagration cannot consume such lots of reactive mixtures. It is also found observed that some unreacted mixtures with low temperatures are ejected from the triple point, which could have a negative effect on the outlet temperature distribution of the combustor.

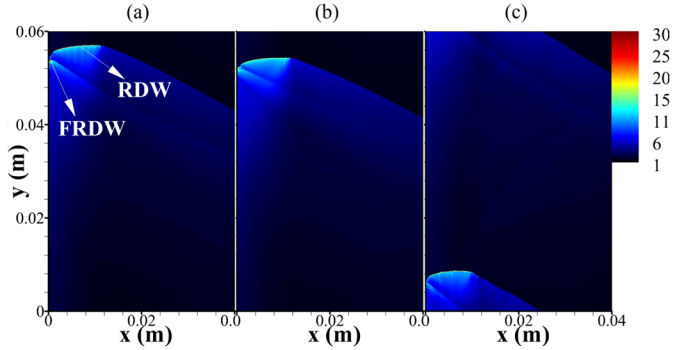

Fig. 9 Instantaneous distributions of pressure (atm) for (a) Case RD (Φ_s = 1.0), (b) Case RDF2 (Φ_s = 1.2), (c) Case RDF3 (Φ_s = 1.4) at the same time.

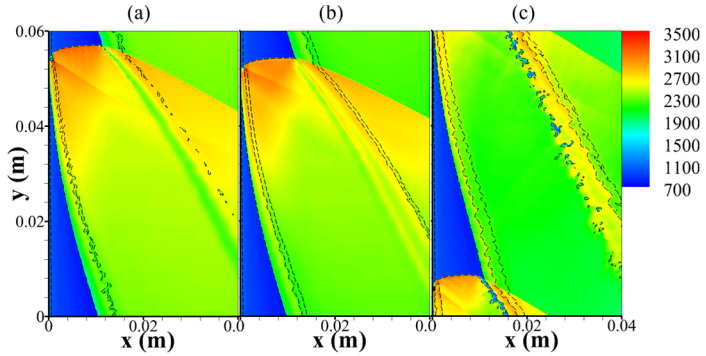

Fig. 10 Instantaneous distributions of temperature (K) for (a) Case RD (Φ_s = 1.0), (b) Case RDF2 (Φ_s = 1.2), (c) Case RDF3 (Φ_s = 1.4) at the same time. Here the black dashed lines refer to fuel mass fraction Y_F = 0.01.

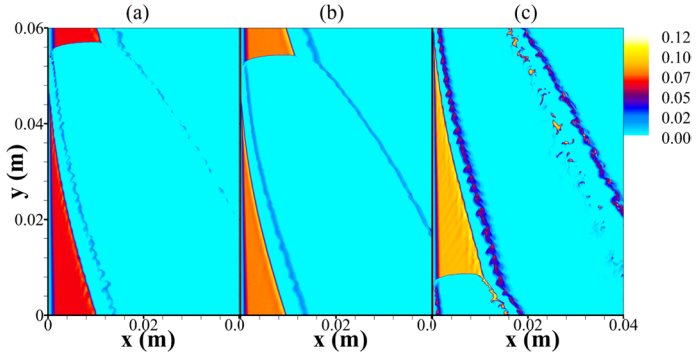

Fig. 11 Instantaneous distributions of fuel mass fraction for (a) Case RD (Φ_s = 1.0), (b) Case RDF2 (Φ_s = 1.2), (c) Case RDF3 (Φ_s = 1.4) at the same time.

The temporal pressure signals from the near-inlet observation point are shown in Fig. 12. The effects of the spray equivalence ratio and the comparison between the gaseous RDW and two-phase RDW with different fuel mass loadings are considered. As depicted in Fig. 12(a), the increasing Φ_s results in a faster propagation velocity of the RDW but a decreasing detonation strength. This is mainly due to the counterbalance between the chemical reaction and droplet-detonation interaction. The increasing fuel droplets contribute to the exothermic reaction from the evaporation to form the reactive mixtures near the inlet, which leads to the acceleration of the detonation propagation. This can be verified in Fig. 8, which shows that the increasing fuel mass leads to an increase in the wave velocity. On the other hand, the large quality of droplets reduces the local temperature and the interaction between the dispersing droplets and the RDW suppresses the detonation pressure, as seen by the comparisons between the gaseous RDW and the two-phase RDW in Fig. 12(c) and Fig. 12(d). The increase in the equivalence ratio is found to have a more obvious influence on the suppression of detonation strength. In addition, the effects of droplets are slight for the stoichiometric mixture, which means that the quasi-balance between the chemical reaction and the droplet-detonation interaction is achieved.

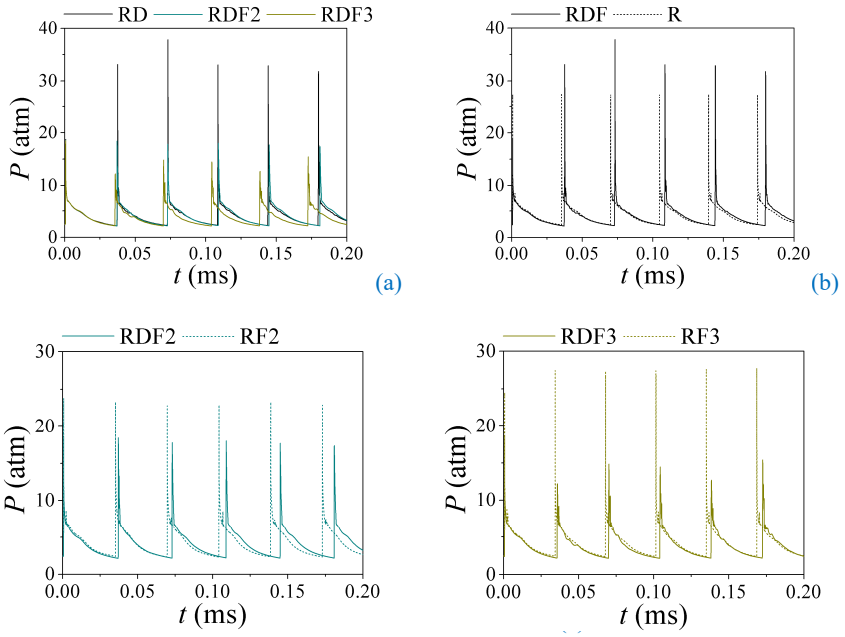

Fig. 12 Variation of pressure at the observation point: (a) various Φ_s, (b) $\Phi_s = \Phi_0 = 1.0$, (c) $\Phi_s = \Phi_0 = 1.2$, and (d) $\Phi_s = \Phi_0 = 1.4$.

For Case RDF1 with a fuel-lean mixture of Φ_s equaling 0.8, the quenching dynamics of the RDW are depicted in Fig. 13 by the temporal pressure distributions. The initial detonation wave is generated in a stoichiometric fuel-air mixture and propagates into the droplet clusters which are injected from the inlet. The decoupling of the shock and flame quickly appears as the detonation wave interacts with the droplets, as illustrated in Fig. 13(b). At the

inlet, a local oblique shock wave replaces the detonation wave. Then the quenching regime expands along the streamwise direction as the RDW propagates towards the transverse direction. The height of the detonation wave becomes short continuously, as depicted from Fig. 13(b) to Fig. 13(e), and the strength of the detonation wave becomes weak. Eventually, the RDW front disappears and it is observed that only a curved shock wave exists in the flow field. Although the detonation wave achieves the stable rotation in the gaseous mixture of Φ_0 = 0.8, the quenching occurs for the same equivalence ratio when detonating fuel droplets. The first reason accounting for this phenomenon is the finite evaporation rates of droplets, which cannot form enough reactive mixtures for the combustion and hence the heat release for supporting the coupling of shock and flame. The other one is attributed to the cooling effect from the droplet evaporation, which decreases the local gas temperature and then reduces the reaction rates. Due to the combined influence, the quenching generates near the injection area of the two-phase mixture and the RDW cannot realize stable operation.

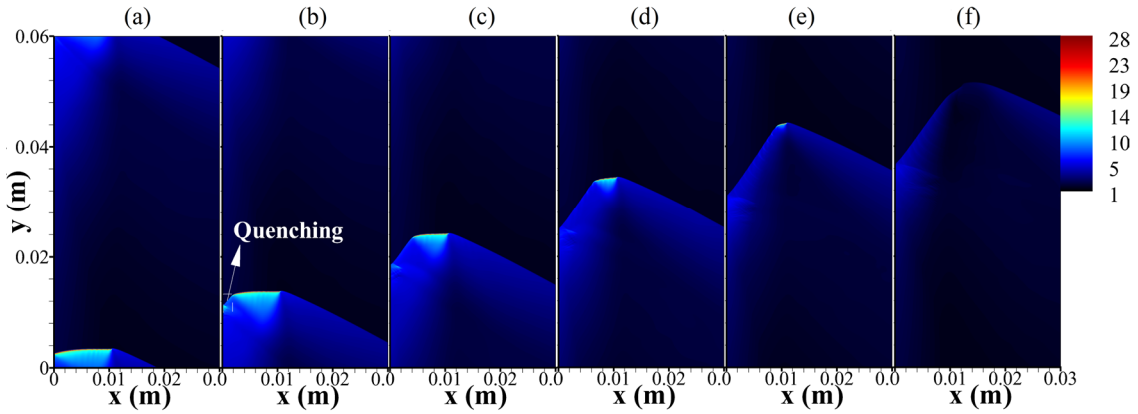

Fig. 13 Temporal evolution of pressure (atm) distribution for Case RDF1 (Φ_s = 0.8): (a) τ_0 μs, (b) τ_0 + 6 μs, (c) τ_0 + 12 μs, (d) τ_0 + 18 μs, (e) τ_0 + 24 μs, and (f) τ_0 + 30 μs.

For the fuel-rich two-phase mixtures, the unstable rotating detonation is found for Case RDF4 as Φ_s increases to 1.6. Fig. 14 and Fig. 15 display the quenching process by the times series of the pressure and temperature, respectively. The initial detonation wave is found to have a single smooth front, as seen in Fig. 14(a). This wave propagates to traverse the fuel-rich mist. Accordingly, the detonation front near the inlet bifurcates to two waves due to the finite droplet evaporation rate. It is found that there are unburned fuel vapors in the downstream area from the FRDW, as indicated by the dashed lines in Fig. 14(b), and the near-inlet gaseous temperature is lower than the temperature in the post-RDW flow, which is due to the reduction of the exothermic reaction. The regime of the unburned reactive mixtures expands as the detonation waves rotate continuously. The front of the RDW becomes corrugated, as shown in Fig. 14(c). This is because the fuel vapors from the droplet evaporation convect

downstream and the chemical reaction burns the fuel-rich mixture, which leads to a slower detonation speed than that from a stoichiometric mixture for the right part of the RDW. The difference in the wave speed results in the wrinkle of the local flame surface, as seen in Fig. 15(c). This enlarges the reaction regime and in turn, increases the consumption rate of the reactive mixture. A local explosion occurs on the RDW surface due to the accelerating chemical reaction around the corrugated area, as indicated by the arrow in Fig. 14(d). Concurrently, it is found that the decoupling of the leading shock and the flame is generated near the inlet due to the unstable detonation, and the unburned pockets have a scattered distribution in the flow after the RDW. The explosion results in two transverse waves that propagate in the opposite directions, as shown in Fig. 14(e). The left-propagating transverse wave (LPTW) ignites the unreacted gas pockets due to the effects of heating and compression and the quenching in Fig. 14(d) disappears due to the re-coupling of the shock and flame. The right-propagating transverse wave (RPLW) burns the local fuel vapors which cross the detonation wave and increase the wave pressure due to the strengthening of the exothermic reaction. The unstable detonation front with cellular wave structures propagates from Fig. 14(f) to Fig. 14(g). In particular, the distance between two neighbor transverse waves becomes close from left to right, associated with the decreasing wave pressure. The temperature distributions of the detonation products are quite non-uniform. The quenching generates from the triple point on the wave front, as depicted in Fig. 14(h). A large quantity of reactive mixtures is not burned and they traverse the front of the RDW, as seen in Fig. 16(d), which further weakens the detonation. The transverse waves are not generated from the triple point and then the transverse waves on the denotation wave front are gradually disappeared. The quenching regime expands from right to left, and the detonation front breaks down finally. The absence of the transverse waves (such as the LPTW and RPTW), associated with their heating and compression effects, results in the quenching of the RDW in the fuel-rich sprays.

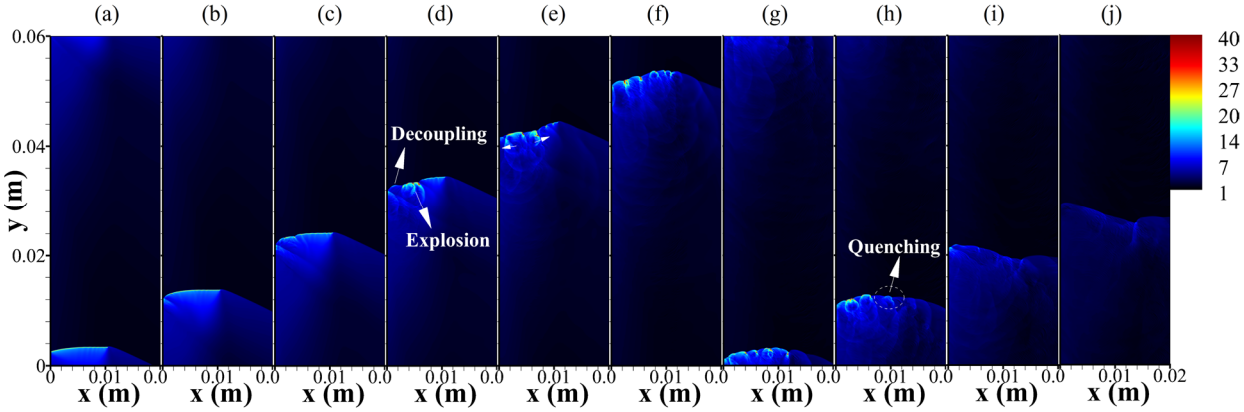

Fig. 14 Temporal evolution of pressure (atm) distribution for Case RDF4 (Φ_s = 1.6): (a) τ_0 μs, (b) τ_0 + 6 μs, (c) τ_0 + 12 μs, (d) τ_0 + 18 μs, (e) τ_0 + 24 μs, (f) τ_0 + 30 μs, (g) τ_0 + 36 μs, (h) τ_0 + 42 μs, (i) τ_0 + 48 μs, and (j) τ_0 + 54 μs.

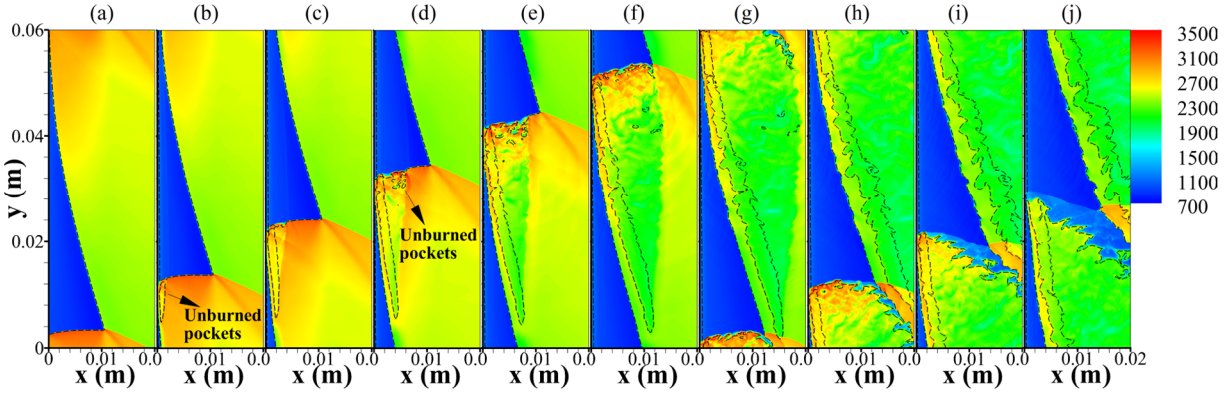

Fig. 15 Temporal evolution of temperature (K) distribution for Case RDF4 (Φ_s = 1.6): (a) τ_0 μs, (b) τ_0 + 6 μs, (c) τ_0 + 12 μs, (d) τ_0 + 18 μs, (e) τ_0 + 24 μs, (f) τ_0 + 30 μs, (g) τ_0 + 36 μs, (h) τ_0 + 42 μs, (i) τ_0 + 48 μs, and (j) τ_0 + 54 μs. Here the black dashed lines refer to fuel mass fraction Y_F = 0.01.

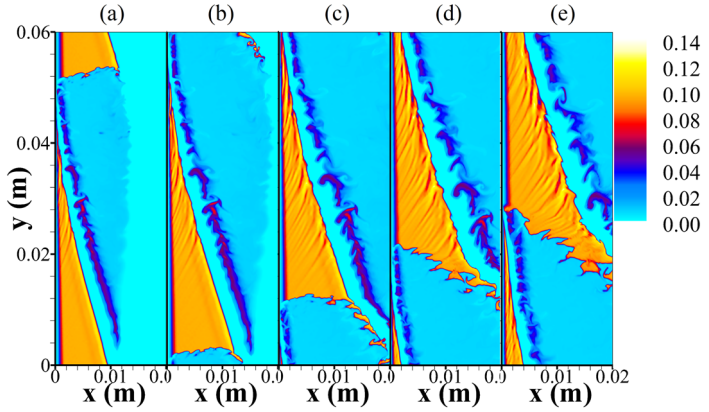

Fig. 16 Instantaneous distribution of fuel mass fraction for Case RDF4 (Φ_s = 1.6): (a) τ_0 + 30 μs, (b) τ_0 + 36 μs, (c) τ_0 + 42 μs, (d) τ_0 + 48 μs, and (e) τ_0 + 54 μs.

The propagation status of the detonation waves under the current conditions is summarized in Fig. 17. It is found that the RDW propagating in a two-phase mixture has a stable regime as the equivalence ratio increases from 1.0 to 1.4. For the RDW fueled with the fuel vapors, the stable region becomes wider for the equivalence ratio varying from 0.8 to 1.6.

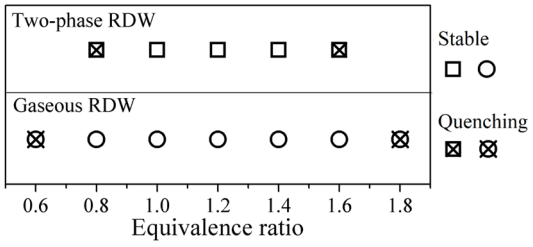

Fig. 17 The propagation status of the detonation waves.

5 Conclusions

A numerical analysis of the kerosene-air two-phase rotating detonation is applied according to the Eulerian-Lagrangian flow model with a two-step reduced chemical mechanism.

The simulations of rotating detonation fueled with pre-evaporated vapors and droplets are performed and the equivalence ratios are varied to study the effects on the rotating detonation stability. For the range of equivalence ratios considered in this analysis, the achievement of stable kerosene-air detonation is more difficult for droplets than for kerosene vapors. Compare with fuel-lean conditions, the RDW tends to be more stable in fuel-rich mixtures with enough fuel supplied for the exothermic reaction.

Within the stable operation regime of the equivalence ratios from 0.8 to 1.6 for the gaseous RDW, the increase of the equivalence ratio results in a faster detonation velocity but an unstable front with cellular wave structures. As the spray equivalence ratio becomes unity, the two-phase RDW realizes the self-sustained propagation. The RDW bifurcates into two waves near the inlet due to the interaction between shock waves, evaporating droplets, and chemical reactions. The increase of Φ_s from 1.0 to 1.4 leads to a faster RDW but a lower detonation pressure. The difference between the gaseous and two-phase RDWs becomes obvious as the equivalence ratio increases.

The quenching mechanism of RDW occurs in either fuel-lean or fuel-rich conditions. For the fuel-lean sprays, the decoupling of the shock and flame is first generated from the inlet, which is attributed to the lack of fuel-air mixtures to sustain the combustion, and the quenching regime expands towards the outlet. For the fuel-rich mixtures, the detonation front becomes unstable with transverse waves. The quenching forms from the triple point and develops to the inlet, owing to the absence of the transverse waves on the RDW front to consume reactive pockets.

Funding

This work is partially supported by start-up funding from Swansea University.

Conflict of interest

The authors report no conflict of interest.

Author contribution

ZX REN wrote and reviewed the manuscript. Y Sun analyzed the results and prepared figures 1-2. B Wang revised and reviewed the manuscript.

References

[1]. Zhao M, Li J M, Teo C J, Khoo B C, Zhang H. Effects of variable total pressures on instability and extinction of rotating detonation combustion[J]. Flow, Turbulence and Combustion, 2020, 104(1): 261-290.

[2]. Bluemner R, Bohon M D, Paschereit C O, Gutmark E J. Experimental study of reactant mixing in model rotating detonation combustor geometries[J]. Flow, Turbulence and Combustion, 2019, 102(2): 255-277.

[3]. Bohon M D, Bluemner R, Paschereit C O, Gutmark E. Measuring rotating detonation combustion using cross-correlation[J]. Flow, Turbulence and Combustion, 2019, 103(1): 271-292.

[4]. Barwey S, Prakash S, Hassanaly M, Raman V. Data-driven classification and modeling of combustion regimes in detonation waves[J]. Flow, Turbulence and Combustion, 2021, 106(4): 1065-1089.

[5]. Yan C, Teng H, Ng H D. Effects of slot injection on detonation wavelet characteristics in a rotating detonation engine[J]. Acta Astronautica, 2021, 182: 274-285.

[6]. Yao S, Tang X, Luan M, Wang J. Numerical study of hollow rotating detonation engine with different fuel injection area ratios[J]. Proceedings of the Combustion Institute, 2017, 36(2): 2649-2655.

[7]. Sato T, Chacon F, White L, Raman V, Gamba M. Mixing and detonation structure in a rotating detonation engine with an axial air inlet[J]. Proceedings of the Combustion Institute, 2021, 38(3): 3769-3776.

[8]. Zhao M, Zhang H. Large eddy simulation of non-reacting flow and mixing fields in a rotating detonation engine[J]. Fuel, 2020, 280: 118534.

[9]. Fotia M L, Hoke J, Schauer F. Study of the ignition process in a laboratory scale rotating detonation engine[J]. Experimental Thermal and Fluid Science, 2018, 94: 345-354.

[10]. Stechmann D P, Sardeshmukh S, Heister S D, Mikoshiba K. Role of ignition delay in rotating detonation engine performance and operability[J]. Journal of Propulsion and Power, 2019, 35(1): 125-140.

[11]. Fujii J, Kumazawa Y, Matsuo A, Nakagami S, Matsuoka K, Kasahara J. Numerical investigation on detonation velocity in rotating detonation engine chamber[J]. Proceedings of the combustion Institute, 2017, 36(2): 2665-2672.

[12]. Wen H, Xie Q, Wang B. Propagation behaviors of rotating detonation in an obround combustor[J]. Combustion and Flame, 2019, 210: 389-398.

[13]. Jourdaine N, Tsuboi N, Ozawa K, Kojima T, Hayashi A K. Three-dimensional numerical thrust performance analysis of hydrogen fuel mixture rotating detonation engine with aerospike nozzle[J]. Proceedings of the Combustion Institute, 2019, 37(3): 3443-3451.

[14]. Liu S J, Lin Z Y, Liu W D, Lin W, Zhuang F C. Experimental realization of H2/air continuous rotating detonation in a cylindrical combustor[J]. Combustion Science and Technology, 2012, 184(9): 1302-1317.

[15]. Wang Y, Wang J. Effect of equivalence ratio on the velocity of rotating detonation[J]. International journal of hydrogen energy, 2015, 40(25): 7949-7955.

[16]. Anand V, George A S, Driscoll R, Gutmark E. Investigation of rotating detonation combustor operation with H2-Air mixtures[J]. International Journal of Hydrogen Energy, 2016, 41(2): 1281-1292.

[17]. Fotia M L, Schauer F, Kaemming T, Hoke J. Experimental study of the performance of a rotating detonation engine with nozzle[J]. Journal of Propulsion and Power, 2016, 32(3): 674-681.

[18]. Deng L, Ma H, Xu C, Zhou C, Liu X. Investigation on the propagation process of rotating detonation wave[J]. Acta Astronautica, 2017, 139: 278-287.

[19]. Xie Q, Wen H, Li W, Ji Z, Wang B, Wolanski P. Analysis of operating diagram for H2/Air rotating detonation combustors under lean fuel condition[J]. Energy, 2018, 151: 408-419.

[20]. Xie Q, Wang B, Wen H, He W, Wolanski P. Enhancement of continuously rotating detonation in hydrogen and oxygen-enriched air[J]. Proceedings of the Combustion Institute, 2019, 37(3): 3425-3432.

[21]. Li B, Wu Y, Weng C, Zheng Q, Wei W. Influence of equivalence ratio on the propagation characteristics of rotating detonation wave[J]. Experimental Thermal and Fluid Science, 2018, 93: 366-378.

[22]. Kindracki J. Experimental research on rotating detonation in liquid fuel–gaseous air mixtures[J]. Aerospace Science and Technology, 2015, 43: 445-453.

[23]. Frolov S M, Aksenov V S, Ivanov V S, Shamshin I O. Continuous detonation combustion of ternary “hydrogen–liquid propane–air” mixture in annular combustor[J]. International Journal of Hydrogen Energy, 2017, 42(26): 16808-16820.

[24]. Frolov S M, Shamshin I O, Aksenov V S, Gusev P A, Zelensky V A, Evstratov E V, Alymov M I. Rocket engine with continuously rotating liquid-film detonation[J]. Combustion Science and Technology, 2018.

[25]. Zheng Q, Meng H, Weng C, Wu Y, Feng W, Wu M. Experimental research on the instability propagation characteristics of liquid kerosene rotating detonation wave[J]. Defence Technology, 2020, 16(6): 1106-1115.

[26]. Zhao M, Wang K, Zhu Y, Wang Z, Yan Y, Wang Y, Fan W. Effects of the exit convergent ratio on the propagation behavior of rotating detonations utilizing liquid kerosene[J]. Acta Astronautica, 2022, 193: 35-43.

[27]. Meng H, Xiao Q, Feng W, Wu M, Han X, Wang F, Weng C, Zheng Q. Air-breathing rotating detonation fueled by liquid kerosene in cavity-based annular combustor[J]. Aerospace Science and Technology, 2022, 122: 107407.

[28]. Xu G, Wu Y, Xiao Q, Ding C, Xia Y, Li Q, Weng C. Characterization of wave modes in a kerosene-fueled rotating detonation combustor with varied injection area ratios[J]. Applied Thermal Engineering, 2022, 212: 118607.

[29]. Cheng P, Wu Y, Song F, Xu S, Chen X, Zhou J, Yang X. Combustion products analysis of large-scale kerosene/air rotating detonation combustor[J]. Combustion Science and Technology, 2022: 1-13.

[30]. Ma Y, Zhou S, Ma H, Ge G, Yu D, Zou G, Liang Z, Zhang T. Experimental investigation on propagation characteristics of liquid-fuel/preheated-air rotating detonation wave[J]. International Journal of Hydrogen Energy, 2022, 47(57): 24080-24092.

[31]. Hayashi A K, Tsuboi N, Dzieminska E. Numerical Study on JP-10/Air Detonation and Rotating Detonation Engine[J]. AIAA Journal, 2020: 1-17.

[32]. Meng Q, Zhao M, Zheng H, Zhang H. Eulerian-Lagrangian modelling of rotating detonative combustion in partially pre-vaporized n-heptane sprays with hydrogen addition[J]. Fuel, 2021, 290: 119808.

[33]. Wang F, Weng C. Numerical research on two-phase kerosene/air rotating detonation engines[J]. Acta Astronautica, 2022, 192: 199-209.

[34]. Salvadori M, Panchal A, Ranjan D, Menon S. Numerical study of detonation propagation in H2-Air with kerosene droplets. AIAA SCITECH 2022 Forum. 2022: 0394.

[35]. Wang J, Lin W, Huang W, Shi Q, Zhao J. Numerical study on atomization and evaporation characteristics of preheated kerosene jet in a rotating detonation scramjet combustor[J]. Applied Thermal Engineering, 2022, 203: 117920.

[36]. Huang X, Lin Z. Analysis of coupled-waves structure and propagation characteristics in hydrogen-assisted kerosene-air two-phase rotating detonation wave[J]. International Journal of Hydrogen Energy, 2022, 47(7): 4868-4884.

[37]. Crowe C T, Sharma M P, Stock D E. The particle-source-in cell (PSI-CELL) model for gas-droplet flows[J]. Journal of fluids engineering, 1977, 99(2): 325-332.

[38]. Poling B E, Prausnitz J M, O'connell J P. The properties of gases and liquids[M]. New York: Mcgraw-hill, 2001.

[39]. Ling Y, Balachandar S, Parmar M. Inter-phase heat transfer and energy coupling in turbulent dispersed multiphase flows[J]. Physics of Fluids, 2016, 28(3): 033304.

[40]. Ren Z, Wang B, Zheng L. Numerical analysis on interactions of vortex, shock wave, and exothermal reaction in a supersonic planar shear layer laden with droplets[J]. Physics of Fluids, 2018, 30(3): 036101.

[41]. Ren Z, Wang B, Xiang G, Zheng L. Effect of the multiphase composition in a premixed fuel–air stream on wedge-induced oblique detonation stabilisation[J]. Journal of Fluid Mechanics, 2018, 846: 411-427.

[42]. Hu X Y, Wang Q, Adams N A. An adaptive central-upwind weighted essentially non-oscillatory scheme[J]. Journal of Computational Physics, 2010, 229(23): 8952-8965.

[43]. Franzelli B, Riber E, Sanjosé M, Poinsot T. A two-step chemical scheme for kerosene–air premixed flames[J]. Combustion and Flame, 2010, 157(7): 1364-1373.

[44]. Schauer F, Miser C, Tucker C, Bradley R, Hoke J. Detonation initiation of hydrocarbon-air mixtures in a pulsed detonation engine[C]. 43rd AIAA aerospace sciences meeting and exhibit. 2005: 1343.

[45]. Austin J M, Shepherd J E. Detonations in hydrocarbon fuel blends[J]. Combustion and flame, 2003, 132(1-2): 73-90.

[46]. Fievisohn R T, Yu K H. Steady-state analysis of rotating detonation engine flowfields with the method of characteristics[J]. Journal of Propulsion and Power, 2017: 89-99.

[47]. Uemura Y, Hayashi A K, Asahara M, Tsuboi N, Yamada E. Transverse wave generation mechanism in rotating detonation[J]. Proceedings of the Combustion Institute, 2013, 34(2): 1981-1989.